CCFE
CULHAM CENTRE FOR FUSION ENERGY

UK Atomic Energy Authority

UKAEA-CCFE-PR(21)77

A. Loarte, A. R. Polevoi, M. Schneider, S.D. Pinches, E. Fable, E. Militello Asp, Y. Baranov, F. Casson, G. Corrigan, L. Garzotti, D. Harting, P. Knight, F. Koechl, V. Parail, D. Farina, L. Figini, H. Nordman, P. Strand, R. Sartori

H-mode plasmas in the Pre-Fusion Plasma Operation 1 phase of the ITER Research Plan

H-mode plasmas in the Pre-Fusion Plasma Operation 1 phase of the ITER Research Plan

A. Loarte, A. R. Polevoi, M. Schneider, S.D. Pinches, E. Fable, E. Militello Asp, Y. Baranov, F. Casson, G. Corrigan, L. Garzotti, D. Harting, P. Knight, F. Koechl, V. Parail, D. Farina, L. Figini, H. Nordman, P. Strand, R. Sartori

This is a preprint of a paper submitted for publication in Nuclear Fusion

H-mode plasmas in the Pre-Fusion Plasma Operation 1 phase of the ITER Research Plan

A. Loarte[1], A. R. Polevoi[1], M. Schneider[1], S.D. Pinches[1] E. Fable[2], E. Militello Asp[3], Y. Baranov[3], F. Casson[3], G. Corrigan[3], L. Garzotti[3], D. Harting[3], P. Knight[3], F. Koechl[3], V. Parail[3], D. Farina[4], L. Figini[4], H. Nordman[5], P. Strand[5], R. Sartori[6]

[1]ITER Organization, Route de Vinon-sur-Verdon, CS 90 046, 13067 St Paul Lez Durance, France

[2]Max-Planck-Insitut für Plasmaphysik, Boltzmannstr. 2, 85748 Garching, Germany

[3]Culham Centre for Fusion Energy, Culham Science Centre, Abingdon, OX14 3DB, UK

[4]Istituto di Fisica del Plasma CNR, 20125 Milano, Italy

[5]Chalmers University of Technology, Göteborg, Sweden

[6]Fusion for Energy Joint Undertaking, Josep Pla 2, 08019, Barcelona, Spain

Abstract

The optimum conditions for access and sustainment of H-mode plasmas and their expected plasma parameters in the Pre-Fusion Operation 1 (PFPO-1) phase of the ITER Research Plan, where the additional plasma heating will be provided by 20 MW of Electron Cyclotron Heating (ECH), are assessed. The assessment is performed on the basis of empirical and physics-based scalings derived from present experiments and integrated modelling of these plasmas including a range of first principle transport models for the core plasma. The predictions of the integrated modelling of ITER H-mode plasmas are compared with ITER-relevant experiments carried out at JET (low collisionality high current H-modes and ASDEX-Upgrade (significant electron heating) for both global H-mode properties and scale lengths of density and temperature profiles finding reasonable agreement. Specific integration issues of the PFPO-1 H-mode plasma scenarios are discussed taking into account the impact of the specificities of the ITER tokamak design (level of ripple, etc.).

1. Introduction

The ITER Research Plan considers the option to investigate H-mode access and sustainment in the initial phase of Pre-Fusion Plasma Operation (PFPO-1) in hydrogen or helium plasmas to minimize scientific and operational risks for later operational phases in the ITER Research Plan [IRP 2018]. Specifically, H-mode operation in PFPO-1 would allow an early determination of the required power to access and sustain H-modes in ITER and provide first evidence of the energy confinement level of H-mode plasmas in ITER, would provide a first characterization of power fluxes to plasma facing components during Edge Localized Modes (ELMs) and would allow a first exploration of edge-core integration operation aspects in H-mode in ITER.

In this phase, the only heating and current drive scheme available in ITER is 20 MW of ECH (170 GHz) and this poses specific restrictions to the H-mode scenario regimes that can be explored in this phase. An operational space for H-mode operation with 20 MW ECH has been identified for a toroidal field value of 1.8 T and the viability of H-mode access and sustainment taking into account the specificities of the heating scheme for this value of the field (3rd harmonic ECH) has been demonstrated for ITER [Schneider 2019].

In this paper, we complement the studies in [Schneider 2019] with more detailed studies of H-mode access and plasma transport modelling and compare the predictions for ITER with experimental results, discuss edge-core compatibility issues and other specific H-mode aspects impacted by specificities of 1.8 T H-mode plasmas in ITER (e.g. impact of H-mode ripple).

The paper is organized as follows: in Sect. 2 we discuss the issues related to H-mode access at 1.8 T in ITER in PFPO-1, in Sect. 3 we present the results of integrated transport modelling of 1.8 T H-mode plasmas in ITER with various first principle models, in Sect. 4 we compare the results of the integrated transport modelling of 1.8 T ITER H-mode plasmas with relevant plasmas from present experiments, in Sect. 5 we discuss edge-core and other integration issues in these plasmas and in Sect. 6 we summarize our studies and draw conclusions.

2. H-mode access at 1.8 T in PFPO-1

The power required to access the H-mode (P_{LH}) is evaluated for ITER on the basis of the ITPA 2008 scaling [Martin 2008]:

$$P_{LH,D} = 0.049 \times \overline{n_e}^{0.72} \times B_t^{0.8} \times S^{0.94} \quad (1)$$

where S is the plasma surface (~ 680 m^2 for ITER plasmas), $\overline{n_e}$ is the line averaged density and B_t is the toroidal magnetic field on the magnetic axis. Note that this scaling is derived from a multi-machine database in deuterium plasmas dominated with devices with carbon plasma facing components. For individual machines it was found that the P_{LH} value provided by Eq. 1 is only applicable above a given density value ($n_{L,H,min}$), for densities under this value P_{LH} is found to increase with decreasing density, i.e. an opposite trend to that predicted by the scaling. The physics determining this minimum value is not yet fully understood. The value of the turnover density as well as the power threshold in the vicinity of this density can depend on the divertor configuration [Andrew 2006, Hillesheim 2016, Maggi 2014], presence of impurities [Takizuka 2004], ion species [McDonald 2010,Maggi 2018, Gohil 2012, Yan 2016] and plasma rotation [Gohil 2008].

To evaluate $n_{L,H,min}$ in ITER we adopt the physics model put forward on the basis of ASDEX-Upgrade [Ryter 2014] that showed that this minimum density is determined by the role of the edge ion heating in triggering the L-H transition. Based on these results, an expression for the density providing the minimum threshold L-H power has been derived for ITER. It should be noted that this physics picture describes well the values found in other tokamaks of different size such as Alcator C-Mod [Schmidtmayr 2018] but for other tokamaks such as JET its applicability is less clear and other physics mechanisms related to the presence of impurities may be at work [Bourdelle 2014, Yan 2016 Hillesheim 2016]. On the basis of the model in [Ryter 2014]:

$$n_{LH,min}^{scal}(10^{20}m^{-3}) \approx 0.07\, I_p^{0.34} B_t^{0.62} a^{-0.95} (R/a)^{0.4} \quad (2)$$

For ITER, this leads to,

$$\frac{n_{LH,min}^{scal}}{n_{GW}} \approx 0.71 \frac{I_p^{0.34} B_t^{0.62}}{I_p} \quad (3)$$

For q_{95} = 3 conditions in ITER, for which B_t (T) = 0.35×I_p (MA), this corresponds to $n_{LH,min}^{scal} \approx 0.35 \times n_{GW}$.

This scaling is derived for deuterium plasmas and thus needs to be adjusted to provide an evaluation of P_{LH} for other isotopes and ion species. For hydrogen plasmas the H-mode power threshold is found to be typically twice that of deuterium $P_{LH,H} = 2 \times P_{LH,D}$, while for helium this is $P_{LH,He} = [1\ to\ 1.5] \times P_{LH\,D}$.

The isotope scaling with ion mass (M) was originally identified in T, DT, D and H experiments at JET, $P_{LH} \propto M^{-1}$ [Righi 1999] and found to be a good guideline in other tokamaks and subsequent JET experiments with the precise value of the multiplier from H to D depending on plasma parameters [Maggi 2018].

He versus D has also been explored on DIII-D, ASDEX-Upgrade, Alcator C-Mod and JET, most of the experiments in a C wall environment [Gohil 2012, McDonald 2010]. When

comparing He with D plasmas, either the power threshold is unchanged (ASDEX-Upgrade), unchanged or somewhat increased depending on density (JET) or largely increased by up to factors of 3 at some densities (DIII-D and Alcator C-Mod). Experiments from JET show that small amounts of H in D plasmas and He in H plasmas can have significant effects on H-mode access [Hillesheim, 2016]. Although this was identified already in ASDEX-Upgrade for He plasmas [Ryter, 2013], the JET results indicate that the issue is more complex and can potentially be beneficially exploited to expand the range of ITER H-mode operation in hydrogen-dominant plasmas. In our further consideration we use the generally conservative assumptions $P_{LH,H} = 2 \times P_{LH,D}$, and $P_{LH,He} = 1.5 \times P_{LH,D}$ for the whole range of densities, assuming that the minimum of threshold corresponds to the density predicted by Eq. (3).

This prediction of the ITER H-mode $n_{LH,min}$ by Eq. 3, based on maximizing ion heat flux over density, has been confirmed by modelling of 5 MA/1.8 T hydrogen and helium L-mode plasmas with ASTRA [Pereverzev 2002]. The density and temperature profiles for two typical L-mode plasmas modelled are shown in Fig. 1 and the resulting ion heat flux for a range of densities is shown in Fig. 2. The density which provides the minimum power for H-mode access, $n_{LH,min}$, has been evaluated on the basis of 1.5-D transport modelling as the density at which the edge ion power flux starts to saturate with increasing density following the physics picture in [Ryter 2014]. The value for $n_{LH,min}$ derived from direct modelling appears to be close to the scaling predictions $n_{LH,min} \approx n_{LH,min}^{scal} \approx 0.35\, n_{GW}$ (Fig. 2). The actual ratio at which the edge power flow saturates depends on assumptions regarding the electron and ion transport (ratio χ_i/χ_e), but the value of the density at which saturation takes place depends only weakly on this assumption, provided that the overall confinement is assumed to follow the L-mode scaling (this is the normalizing parameter for the actual values of χ_i and χ_e). It should be noted that these ASTRA simulations also show a clear difference on the maximum value of the edge ion heat flux for hydrogen and helium plasmas but a weak dependence of the minimum density at which this heat flux saturates on plasma species (H or He). Both these predictions are presently the topic of on-going experimental and modelling R&D [Solano 2019].

The predicted value of $n_{LH,min}$ for ITER plasmas at 1.8 T spanning a range of q_{95} = 3-6 is shown in Fig. 3; as can be seen in this figure very low absolute values of plasma density 1.0-2.0 10^{19} m^{-3} are characteristic of these H-mode plasmas. The corresponding H-mode power threshold value at this minimum density and at $n_e = 0.5\, n_{GW}$ for hydrogen and helium plasmas (assuming the higher range of the power threshold for helium) is shown in Fig. 4. For sustained H-mode operation in ITER, it is likely that the plasma density will be higher than this minimum value due to the reduced transport in the pedestal. Thus, in order to estimate the power required for sustained H-mode operation of 1.8 T plasmas, a value of $\langle n_e \rangle = 0.5\, n_{GW}$ has been used; this accounts for the potential increase of the plasma density from the minimum value after the L-H transition to stationary H-mode conditions. For 5 MA operation at 1.8 T sustained H-modes, operation in helium plasmas requires $P_{sustained}^{He\ H-mode} \sim$ 16 MW while for hydrogen plasmas $P_{sustained}^{H\ H-mode} \sim$ 23 MW is required. Given the baseline ECH installed power of 20 MW in this phase, sustained operation in He plasmas is expected to be viable, although with a reduced margin of power flow above the threshold $P_{tot}/P_{LH} \sim 1.3$. For hydrogen plasmas the H-mode may be accessible since $P_{LHmin}^{H} \sim$ 17.5 MW but sustained H-mode operation is unlikely. On this basis, the possibility for an early upgrade of the ITER ECH system to provide 30 MW already in PFPO-1 is presently under discussion [Schneider 2019]. This increased ECH power would provide robust sustain helium plasma H-mode operation and the possibility to explore hydrogen plasma H-modes, and/or hydrogen-dominant plasmas (with 10 % helium) if the H-mode threshold is reduced by the presence of helium as found at JET [Hillesheim 2016] for 5 MA/1.8T plasmas in ITER. Note that the margin to P_{LH} can be increased at 1.8 T by operating at lower current, e.g. at 3.3 MA with q_{95} = 4.5. However, the increase in margin for sustained

operation by this approach is very moderate since, from Eqs. (1) and (3), $P_{LH}\left(n_{LH,min}^{scal}\right) \sim I_p^{0.24}$, and, in addition, issues related to unabsorbed power due to the 3rd harmonic heating become more problematic due to the decrease in density and temperature of the plasmas so that the approach to increase the H-mode operational space by I_p reduction under 5 MA for 1.8 T hydrogen and helium plasmas is not viable, in practice, in PFPO-1.

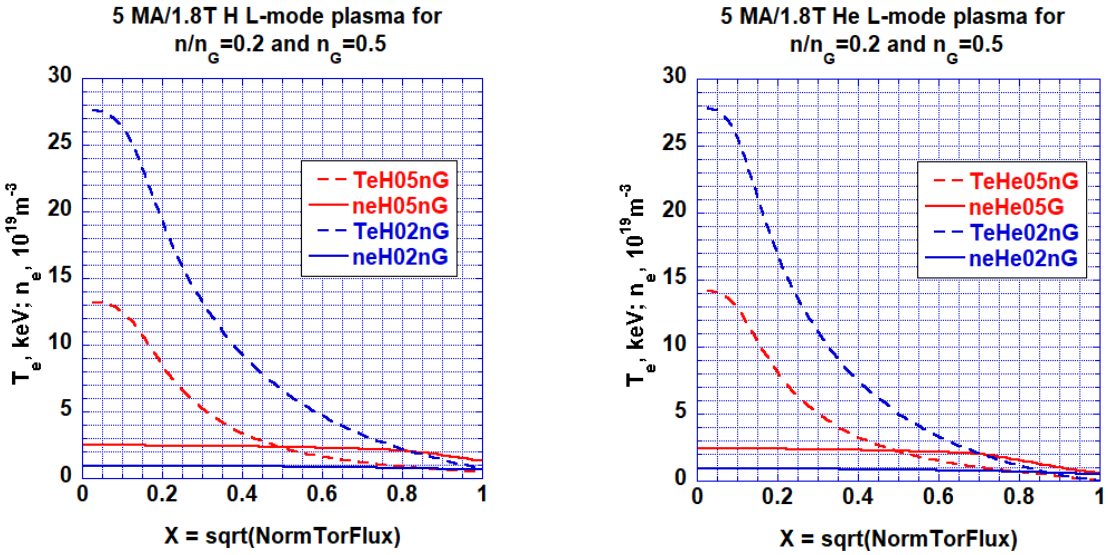

Figure 1. Density and temperature profiles of 5MA/1.8T hydrogen L-mode plasmas with 20 MW of ECH at two values of plasma density (n/n_{GW} = 0.2, 0.5): a) hydrogen plasma, b) helium plasma.

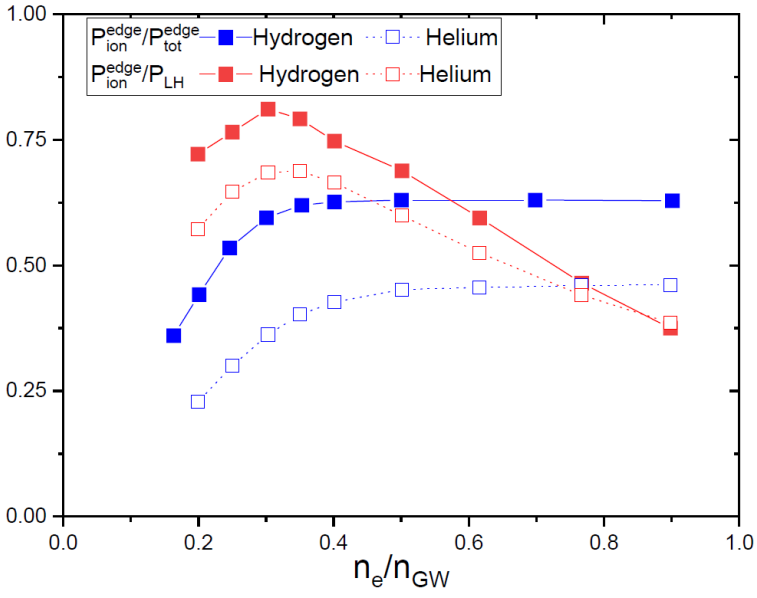

Figure 2. Fraction of the ion edge power flow to the total edge power and to the L-H threshold power versus density (normalized to the Greenwald density) for 5 MA/1.8T plasmas with 20 MW of ECRH heating in hydrogen and helium.

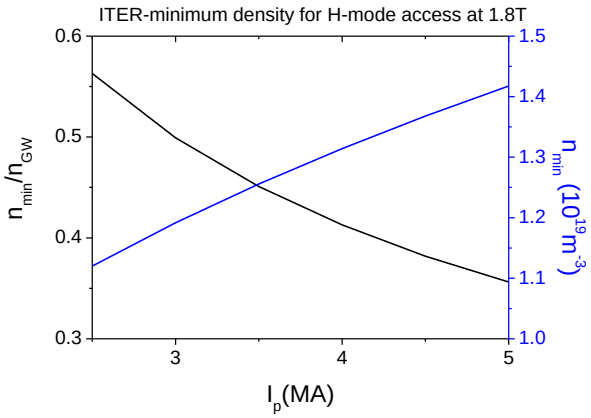

Figure 3. Predicted minimum density for H-mode access in ITER 1.8 T plasmas versus plasma current in absolute value and as a ratio to the Greenwald density.

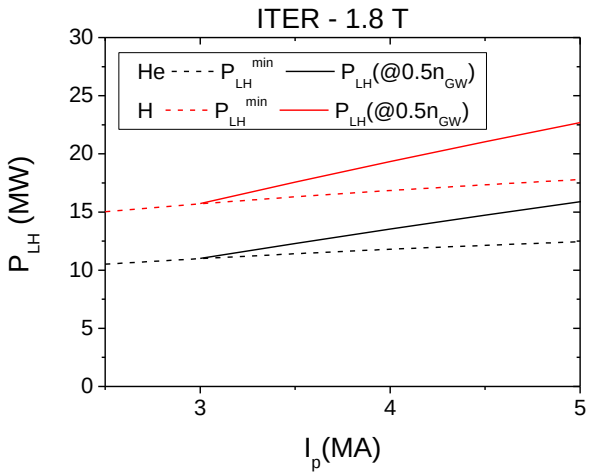

Figure 4. Power required to access the H-mode at $n = n_{LH,min}$ and to sustain H-mode plasmas (at $n = n_{GW}/2$) for 1.8 T plasmas in ITER H and He plasmas.

ITER is equipped with ferromagnetic inserts to reduce the value of the toroidal field (TF) ripple; the mass of these inserts is optimized to reduce the value of TF ripple from 1.0% down to 0.3% at the separatrix outer midplane in ITER for an axial vacuum toroidal field value of 5.3 T. Thus, the level of ripple at 1.8 T is sizeable for the nominal outer midplane separatrix position (1.3 %) since the ferromagnetic inserts overcompensate the natural ripple of ITER determined by its 18 TF coils. This sizeable TF ripple value is not expected to have a significant effect on the power required to access the H-mode or if it has, it is most likely to be favourable (reducing power threshold). The effect of TF ripple on H-mode threshold was found to be negligible at JET for values of the TF ripple spanning from 0.08% up to 1.1% [Andrew 2008]. On the other hand, in JT-60U, the H-mode power threshold was reduced when increasing the ripple [Tobita 1995].

3. Integrated modelling of ITER 5 MA/1.8T H-mode plasmas with models based on first principles

Modelling of 5 MA/1.8T H-mode plasmas with 20 and 30 MW of ECH heating has been performed with the ASTRA integrated modelling suite [Pereverzev 2002] and a range of first principle models for anomalous transport, namely GLF23 [Waltz 1997] and TGLF [Staebler 2007], the latter with two implementations (SAT-0 and SAT-1) including the most up to date one that accounts effects of multi-scale physics on turbulent transport (SAT-1) [Staebler 2017].

An issue identified in applying such first principle models is that the saturation rules used to evaluate plasma transport in the quasilinear approximation are based on gyrokinetic simulations for deuterium plasmas. Therefore, in order to be consistent with the physics models used, the simulations have been performed for D plasmas while the corresponding plasmas in PFPO-1 will be performed in H and He. The development of turbulent transport models that account for isotopic and plasma species effects remains an open R&D issue and further ITER modelling with turbulent transport models that include these effects are planned in the near future.

The simulations have been performed by applying similar modelling assumptions to those in previous ITER studies for DT plasmas [Polevoi 2017] regarding pedestal MHD stability and SOL conditions based on the EPED1+SOLPS boundary condition approach. A simple model for the ECH deposited power has been taken with all radio-frequency power centrally deposited $\rho_{tor} \leq 0.4$ in the electrons, which is a reasonable approximation to the expected ECH power deposition profile for 3rd harmonic heating in these plasma conditions [Schneider 2019]. The density targeted for the simulated plasmas is $n_e/n_{GW} \sim 0.5$. However, the level of density in the plasma is the result of transport and fuelling sources resulting from the application of SOLPS boundary conditions. The results obtained for the density and temperature profiles are shown in Figs. 5 and 6. The particle sources have not been fine-tuned to match the same density level in all simulations causing some variation of the line average density value across the simulations.

Note that sawteeth are not included in these simulations. The application of ECH/ECCD has been proven to have a significant effect on sawtooth frequency depending on the details of the current drive deposition profile (e.g. [Chapman 2012]). The evaluation of these effects for 5 MA/1.8 T ITER plasmas and the resulting sawtooth frequencies requires a detailed assessment that will be the topic of future studies. In this respect, the temperatures modelled in these studies can be considered as an upper limit to those that will be observed in these ITER plasmas.

In general, for all transport models used, electrons and ions are not well coupled thermally in the central part of the plasma. For TGLF, the central ratios of T_e/T_i can be even larger than 3.0 for high heating ECH powers; this is accompanied by a large plasma transport that flattens the density and ion temperature profiles (in part this is responsible for the large central T_e/T_i ratio). The exact magnitude of the ion temperature flattening is to some degree dependent of the implementation of the ion heat diffusivities derived from the TGLF modelled fluxes in the ASTRA transport equations, but the density profile resembles the experimental observations of density pump-out from the centre with strong ECH heating seen in some conditions for present tokamaks [Angioni 2009].

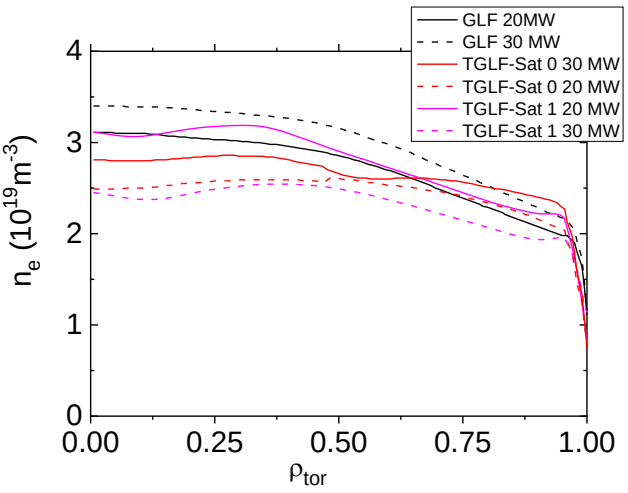

Figure 5. Plasma density profiles for 20 and 30 MW ECH heating power level for ASTRA simulations with three models for anomalous transport GLF23, TGLF not including multi-scale effects (SAT-0 saturation rule) and including multi-scale effects (SAT-1 saturation rule).

a)

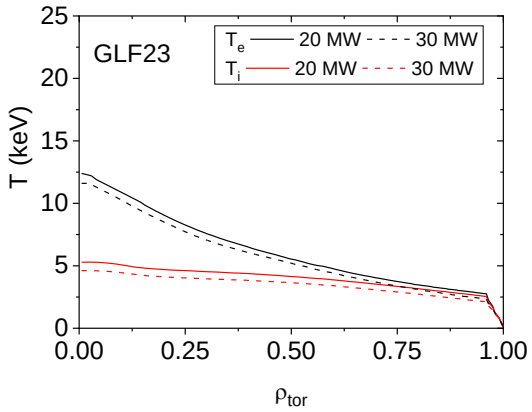

b)

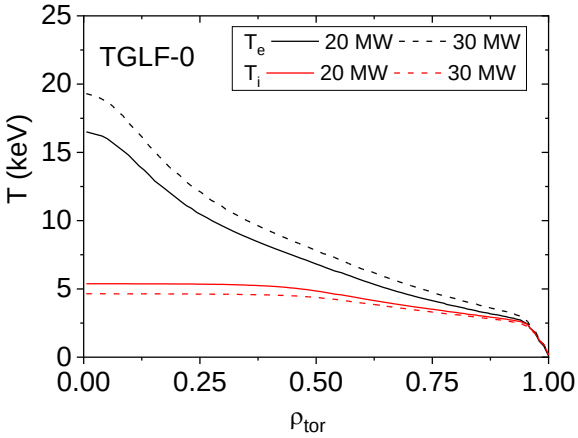

c)

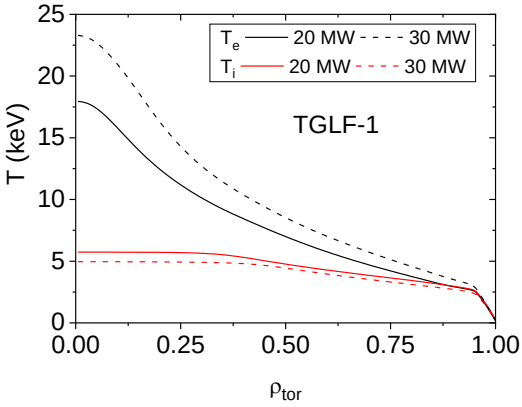

Figure 6. Plasma electron and ion temperature profiles for 20 and 30 MW of central ECH heating power for ASTRA simulations with three models for anomalous transport: (a) GLF23, (b) TGLF not including multi-scale effects (SAT-0 saturation rule) and (c) TGLF including multi-scale effects (SAT-1 saturation rule).

4. Comparison between integrated modelling of ITER 5 MA/1.8T H-mode plasmas and experimental results

To determine if the results obtained represent a well-founded physics-based extrapolation from present experimental results to ITER, we have compared the results of ITER modelling with results from present experiments both in a global and in a local way. In particular, we have compared the modelled density and temperature profiles to determine if the predicted density and temperature gradients match with existing experiments. For these comparisons, we have considered published results from JET high current/low collisionality H-mode for the global comparisons [Nunes 2013] and from dominantly electron heated H-mode plasmas from ASDEX-Upgrade [Sommer 2015].

The overall plasma density and temperature profiles predicted for ITER 5 MA/1.8T ECH heated H-modes have been compared with those from JET H-mode plasmas at similar current

levels (I_p > 4 MA) from [Nunes 2013] with high plasma energy ($W_{plasma,JET}$ ~ 10 MJ compared to $W_{plasma,ITER}$ ~ 30 MJ). We have used a similar approach to scale the JET plasmas to ITER as that followed in pedestal similarity experiments [Beurskens 2009]. We have assumed that β_{ped} will be the same for these JET and ITER plasmas and scaled first the whole density and temperature plasma profiles from JET to ITER accordingly ($n \sim a^{-1/3}B_t^{4/3}$ and $T \sim a^{-1/3}B_t^{2/3}$). Then we have rescaled the density profile to match the value of the pedestal density to that in ITER modelling results while maintaining the same plasma β_{ped}. The outcome of such a scaling comparison is shown in Fig. 7 for both GLF23 and TGLF-SAT-1 modelling results. Although the separate gradients of T_e and T_i are very different for the extrapolated JET plasma and those of the ITER plasmas, the average (T_e+T_i) profiles obtained from the ITER modelling results and those scaled from JET to ITER match rather well. The difference of the individual profiles can be understood because of the different heating systems in these two plasmas. The original JET plasma scaled to ITER (Pulse No. 79676 4.3 MA/3.4 T) is NBI heated (22 MW) and with large electron-ion equipartition while the modelled ITER plasma is electron heated with low equipartition in the plasma core region. It is important to note that the scaling methodology applied could not be simpler; a single point in the whole plasma cross section is used to scale the JET plasmas to ITER. In addition, there are some differences regarding plasma shape between this JET plasma and that modelling for ITER; the plasma triangularity of the JET plasmas (δ ~0.3) is lower than that of the ITER plasma (δ ~ 0.5), which results in a lower pedestal pressure being extrapolated to ITER on the basis of the JET plasma.

a)

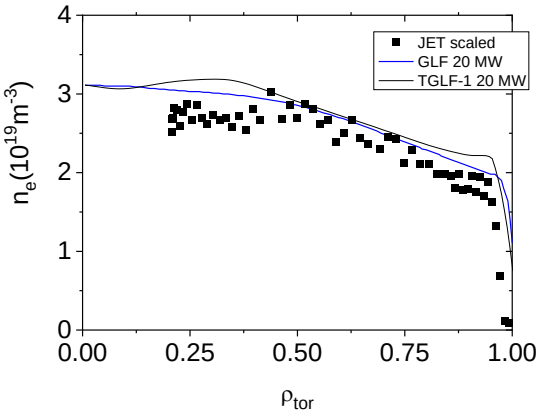

b)

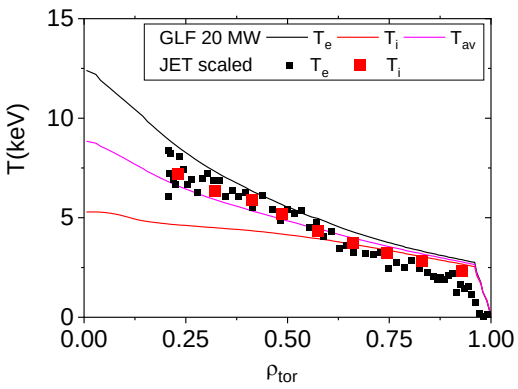

c)

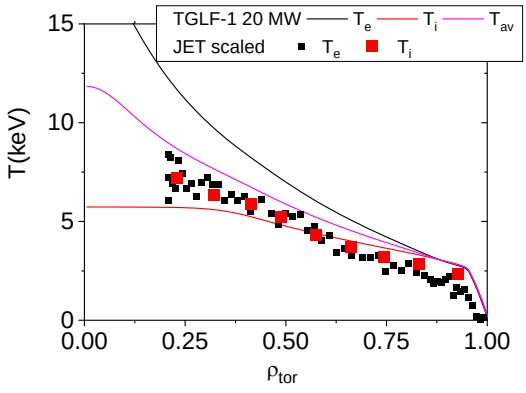

Figure 7. Plasma electron density (a) and electron and ion temperature profiles for 20 MW central EC heating power for ASTRA simulations with for two models for anomalous transport (b) GLF23 and (c) TGLF including multi-scale effects (SAT-1 saturation rule) for ITER 5

MA/1.8 T H-mode plasmas compared with JET [Nunes 2013] high I_p H-mode plasma parameters (Pulse No. 79676 4.3 MA/3.4 T) scaled to ITER; T_{av} = ½ (T_e+T_i).

The plasma density, electron and ion temperatures scale lengths, and the ratios between the latter, for the modelled ITER 5MA /1.8 T plasmas, shown in Fig. 8, have been compared with those from H-mode plasmas in ASDEX-Upgrade with a significant fraction of ECH power in the total auxiliary heating. For this purpose, the density and temperature profiles and the radial scale lengths of plasma density and electron and ion temperatures at mid-radius in ASDEX-Upgrade H-mode experiments [Sommer 2015] have been compared with the values modelled for ITER at the same normalized radial location. In the ASDEX-Upgrade experiments the ratio of electron to ion heating was varied by scanning the ECH to NBI power at constant auxiliary power level up to $P_{ECH}/P_{aux,tot}$ ~ 45%. The satisfactory agreement between the ITER modelling results and those from ASDEX-Upgrade is shown in Figs. 9 and 10. The main difference between ITER modelling and the ASDEX-Upgrade experiments corresponds to the results with GLF that produces much flatter T_i profiles at mid-radius in ITER than in experiment, which is compensated by steeper T_i profiles further inwards towards the plasma centre. This finally leads to a somewhat lower T_e/T_i ratio at the plasma centre with GLF23 than would be expected for purely electron heated plasmas on the basis of the ASDEX-Upgrade data. It should be noted, however, that in the ASDEX-Upgrade experiments the plasmas with higher ECH heating power still were dominated by NBI heating (55% NBI and 45% ECH power) and, thus, these plasmas had significant ion heating unlike the ITER H-mode plasmas modelled here, which are purely electron heated. This is consistent with the higher T_e/T_i ratios at the plasma centre and the lower ion temperature scale lengths predicted by TGLF for ITER plasmas compared to those in ASDEX-Upgrade.

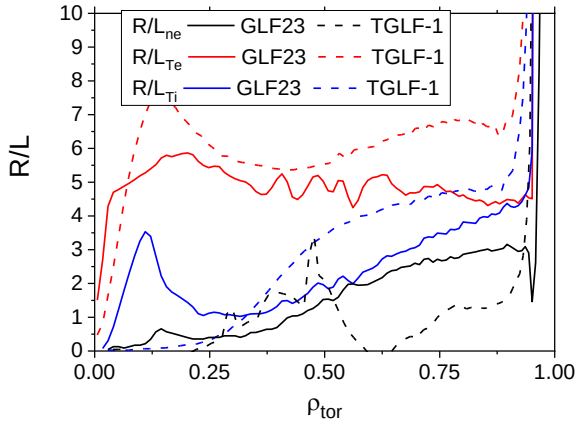

Figure 8. Inverse scale-lengths of the plasma density and electron and ion temperatures for 20 MW central EC heating power level simulated by ASTRA for 5MA/1.8T ITER operation with two models for anomalous transport: GLF23 and TGLF including multi-scale effects (SAT-1 saturation rule) (see Figs. 5, 6).

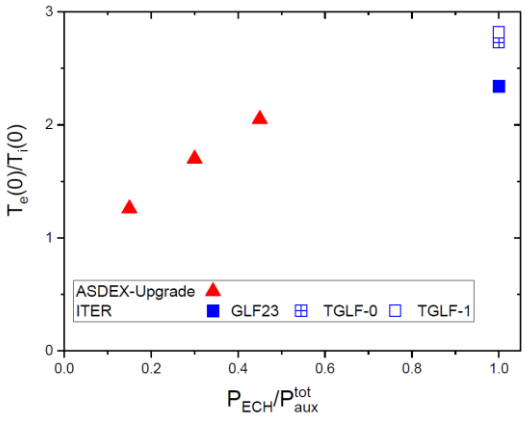

Figure 9. Ratio of the electron to ion temperature at the magnetic axis versus fraction of ECH in total auxiliary power for experiments in ASDEX-Upgrade [Sommer 2015] and for the ITER simulations in Figs. 5 and 6 with 20 MW of ECH power.

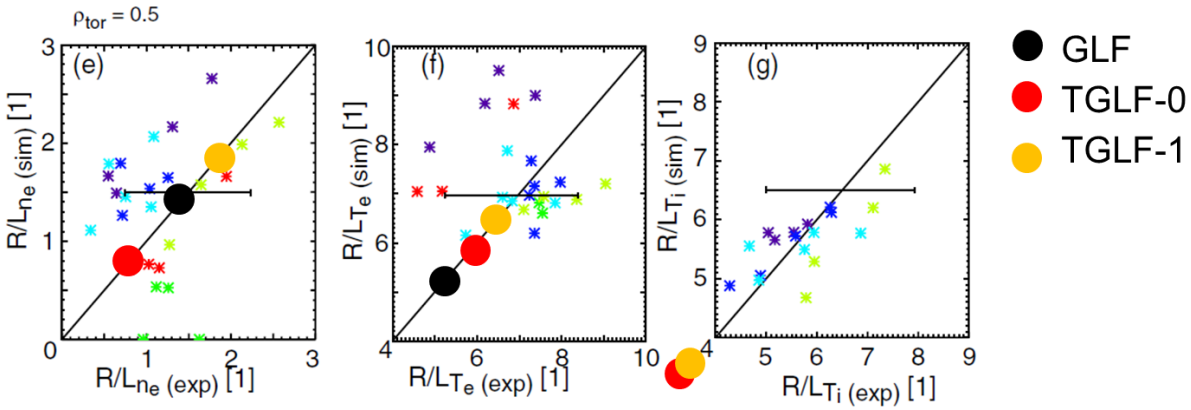

Figure 10. Plasma density and electron and ion temperature normalized inverse scale lengths at mid-radius for ASDEX-Upgrade (model versus experiment comparison) [Sommer 2015] and for the ITER ASTRA simulations in Figs. 5 and 6 with 20 MW of ECH. The normalized inverse scale length for the ion temperature with GLF23, is $R/L_{Ti} \sim 2$.

5. Integration issues for ITER 5 MA/1.8T H-mode plasmas

As mentioned in the introduction, H-mode operation in the PFPO-1 phase of the ITER Research Plan (IRP) has as main objective the reduction of risks for latter phase of the IRP. This concerns aspects related to H-mode access, sustainment and determination of H-mode confinement in ITER as well as the development of control schemes to integrate core and edge plasma aspects which are essential for later phases of the research plan with higher levels of plasma heating, in particular when high levels of alpha heating will be demonstrated in the Fusion Power Operation Phase (FPO). In this respect, it is important to evaluate specific aspects of 1.8 T operation in ITER that can affect H-mode confinement as well as the expected transient and stationary power fluxes to the plasma facing components. On one hand, in order to develop control schemes for these power fluxes, it is interesting that these fluxes are representative of later operational phases. On the other hand, it would be preferable that these loads do not exceed material limits (e.g. melting of tungsten divertor mono-blocks) while the required control schemes are being developed.

Regarding the achievable H-mode confinement, beyond the modelling assessment discussed in the previous two sections, there is a specific issue which is expected to affect H-mode confinement and that is the relatively high level of ripple at the nominal outer midplane separatrix of 1.3% for 1.8 T plasmas in ITER. An assessment of the effects of TF ripple on H-

mode plasmas was jointly performed by coordinated experiments at JET and JT-60U [Saibene 2008, Urano 2011]. The outcome of these experiments was that the value of TF ripple at the level of ~1.3% can have an effect on the pedestal pressure and maximum energy confinement that can be achieved in H-mode with this effect being more significant for low collisonaility plasmas. This corresponds to the JET 2.6 MA plasma as with the pedestal collisionality is ν^*_{ped} ~ 0.04 shown in Fig. 11 from [Urano 2011]. Extrapolation of these findings requires a complete physics-based approach, which is not yet fully developed. If we assume that pedestal collisionality is the key parameter to quantify the effect of ripple on H-mode pedestal behaviour and confinement, we can then use the ITER predictions for the pedestal pressure derived from EPED1+SOLPS [Polevoi 2017], applied to the modelling in Sect. 3, to evaluate the possible effects of increased TF ripple on the pedestal plasma and H-mode confinement for 5MA/1.8T plasmas in ITER. We first evaluate the expected characteristics of the pedestal parameters and H-mode confinement without ripple effects and then consider how they could be modified by the level of TF ripple expected in 5MA/1.8T plasmas in ITER.

According to the EPED1+SOLPS scaling $\nu^*_{ped} \approx 0.16\ (n_{ped}/n_{GW})^3 B^{-0.68}$ [Polevoi 2018], the collisionality of 1.8 T plasmas with the same n_e/n_{GW} be about two times larger than that of B = 5.3 T plasmas. However, for the expected plasma conditions in ITER 5 MA/1.8T plasmas, as discussed in Sects. 2 and 3, we require much lower n_e/n_{GW} values to access and sustain the H-mode (i.e. $n_{ped}/n_{GW}|_{5MA} \sim 0.5\ n_{ped}/n_{GW}|_{15MA\text{-}Q=10}$) with the available heating power level in PFPO-1. This reduces the pedestal plasma collisionality so that, for the foreseen ITER 5 MA/1.8T H-mode plasmas to be explored in PFPO-1, is $\nu^*_{ped}|_{5MA\text{-}PFPO\text{-}1} = 0.25\ \nu^*_{ped}|_{15MA\text{-}Q=10}$. Therefore, ripple effects on pedestal plasma and H-mode confinement are expected to be similar for 5 MA/1.8T PFPO-1 H-mode plasmas that those for Q = 10 plasmas without ferromagnetic (which have ~ 1% ripple). On the basis of the JET experiments [Saibene 2008, Urano 2011] carried out to evaluate the effects TF ripple on Q = 10 plasmas, this implies a reduction of pedestal pressure and H-mode energy confinement by 20-30% compared to the modelling in Sect. 3, which intrinsically assumes no ripple effects. Since this is a significant reduction, alternative magnetic configurations have been developed for 5MA/1.8T plasmas in which the TF ripple at the outer separatrix midplane can be decreased to 0.5 % by reducing the plasma minor radius and shifting the plasma inwards, away from the TF coils, while maintaining good vertical stability control [Lukash 2017].

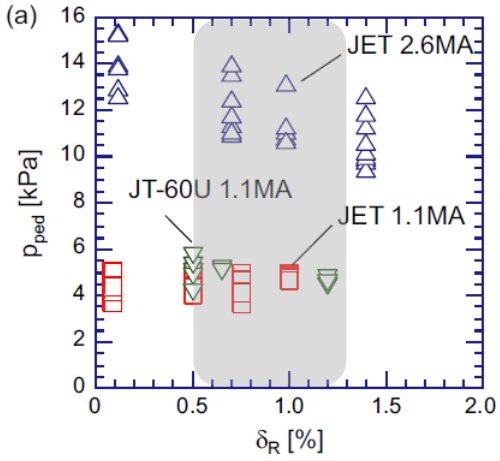

Figure 11. Pedestal plasma pressure versus toroidal ripple level at the outer midplane separatrix for two levels of plasma current at JET compared to JT-60U for the lower current level [Urano 2011]. The vertical scatter corresponds to plasmas with various levels of gas puffing; the upper level of pressure for the 2.6 MA JET plasmas corresponds to a pedestal collisionality of ν^*_{ped} ~

0.04. The band in the figure corresponds to the range of outer separatrix ripple values that can be achieved for 5 MA/1.8 T plasmas in ITER by modifying the magnetic configuration.

Concerning other pedestal related issues, the TF ripple has been found to affect the ELM energy losses both in JET [Saibene 2008] as well as in JET [Aiba 2011] independently of whether TF ripple affects pedestal pressure or not. On this basis, it is expected that ELM energy losses for 5 MA/1.8 T plasmas for the nominal separatrix position with 1.3% ripple will be a factor of 2 lower than predicted from multi-machine scalings from experiments with low ripple values [Loarte 2003]. However, it should be noted that the reduction of ELM energy losses is also correlated with a decrease of edge toroidal rotation with increasing ripple and associated fast ion losses, which are seen at JET [Urano 2011] and JT-60 U [Aiba 2011]. If fast ion loss is the dominant mechanism behind the ELM energy loss reduction with increasing ripple, then this reduction may not materialize for 5 MA/1.8T H-mode plasmas in PFPO-1 since these are ECH heated and there are no fast ions.

Closely related to the ELM energy losses, one of the objectives of H-mode operation at 5 MA/1.8 T in PFPO-1 is to explore ELM control to refine the schemes applied for later operational phases [Loarte 2014]. During PFPO-1, active ELM control can be explored by pellet injection [Polevoi 2003, Futatani 2014] and vertical plasma oscillations [Artola 2018]; in the present formulation of the ITER staged approach [Bigot 2019] the ELM control coils will not operate in this phase. Evaluations on the application of ELM control coils in the PFPO-1 phase have been performed [Li 2020] in the context of discussions that might eventually lead to the advanced installation of the power supplies (all or a partial set) for the ELM control coils to be operational for PFPO-1. Since it will not be possible to demonstrate ELM control from the first 5 MA/1.8T H-mode discharges and the operational space in these conditions is very restricted in PFPO-1, it is important to ensure that uncontrolled ELM power fluxes to the divertor will not exceed material limits (melting of tungsten macro-brushes edges and top surface). This has been the subject of specific studies described in [Gunn 2017] which show that, even for the more conservative estimates of ELM power fluxes at the ITER divertor derived from experimental scalings [Eich 2017], the ELM energy fluxes expected for 5 MA/1.8 T H-mode plasmas are a factor of 1.5 lower than those required to cause tungsten melting of the edge macro-brushes and a factor of 5 lower than those required to cause top macro-brush melting. Integrated simulations of ITER plasmas, considering tungsten production by ELMs and transport into the pedestal plasma in a simplified way, have shown that, although divertor melting is not expected to occur for these plasmas, a basic level of ELM control may be required to prevent H-L transitions due to excessive core tungsten radiation following the ELMs. This is the result of physical sputtering at the tungsten target by the high temperature pedestal ions released by the ELM and its propagation into the core plasma. These tungsten- caused H-L transitions is found to occur at values of ELM energy losses of ~ 1.25 MJ [Polevoi 2018], while the uncontrolled ELM energy is expected to be in the range of ~ 1.5-3 MJ for 5MA/1.8T ITER plasmas on the basis of empirical scalings [Loarte 2003]. It should be noted that the evaluation of core tungsten radiation following ELMs is subject to large uncertainties, in particular related to the fraction of prompt tungsten re-deposition during the ELMs. The assumptions in [Polevoi 2018] to derive the 1.25 MJ ELM energy limit are very conservative (zero prompt re-deposition during the ELM).

Similarly, control of divertor power fluxes by radiative divertor conditions will be explored in these plasmas with the purpose of initial testing of these schemes in H-mode plasmas, in which divertor power flux control is particularly challenging for devices with tungsten divertors [Kallenbach 2013]. Initial integrated modelling of these plasmas has been performed with JINTRAC including: core plasma transport with the EDMW transport model [Strand 2004] for main ions and impurities and the interactions of the plasma with the beryllium first wall and tungsten divertor. The effect of ELMs was simulated with a continuous ELM model by which the transport in the pedestal and near SOL regions is increased to keep the plasma pressure at

MHD stability limit [Militello-Asp 2018]; this approach aims to describe the ELM-averaged behaviour of the pedestal plasma and strictly applies when ELM energy losses are very small. The simulations also include neon that allows the study of radiative divertor regimes.

The results of the core and divertor plasma parameters obtained for two simulations of 5 MA/1.8T hydrogen H-mode plasmas with 30 MW ECH and different Ne puffing levels (10^{19} s^{-1} and 3 10^{19} s^{-1}) are shown for the core plasma profiles in Fig. 12 and for the inner and outer divertor profiles in Fig. 13. For the low Ne rate the effect of Ne on the plasma parameters is negligible, since Ne divertor radiation is 3 MW and less than 0.5 MW is radiated in the core plasma, while for the high rate it is more significant (7 MW of divertor radiation and 1.5 MW of core radiation).

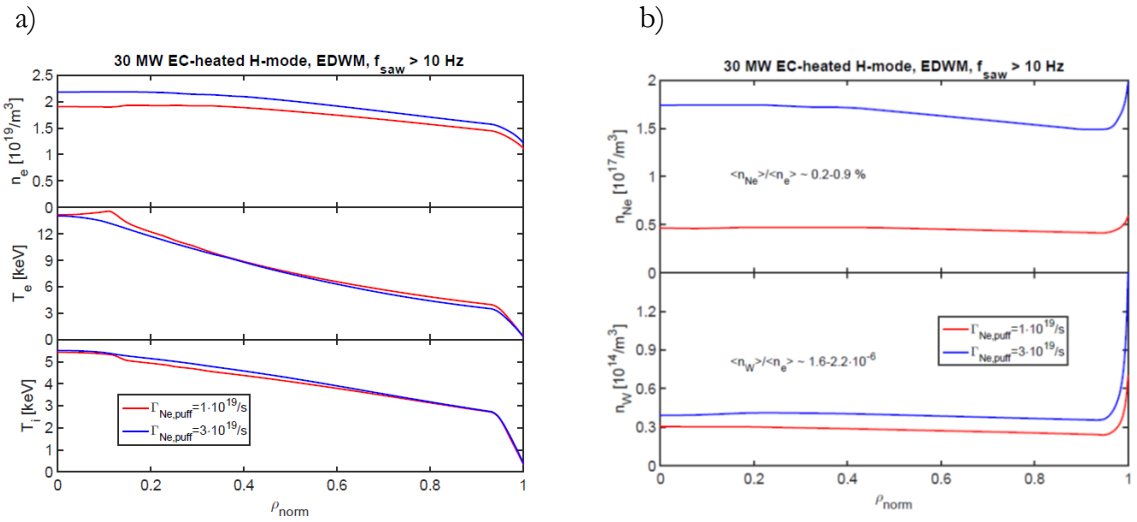

Figure 12. (a) Density and electron and ion temperature profiles and (b) Neon and tungsten profiles in the core plasma for the JINTRAC simulations of 5 MA/1.8T hydrogen H-mode plasmas with the EDMW transport model [Militello-Asp 2018] with 30 MW of the central ECH.

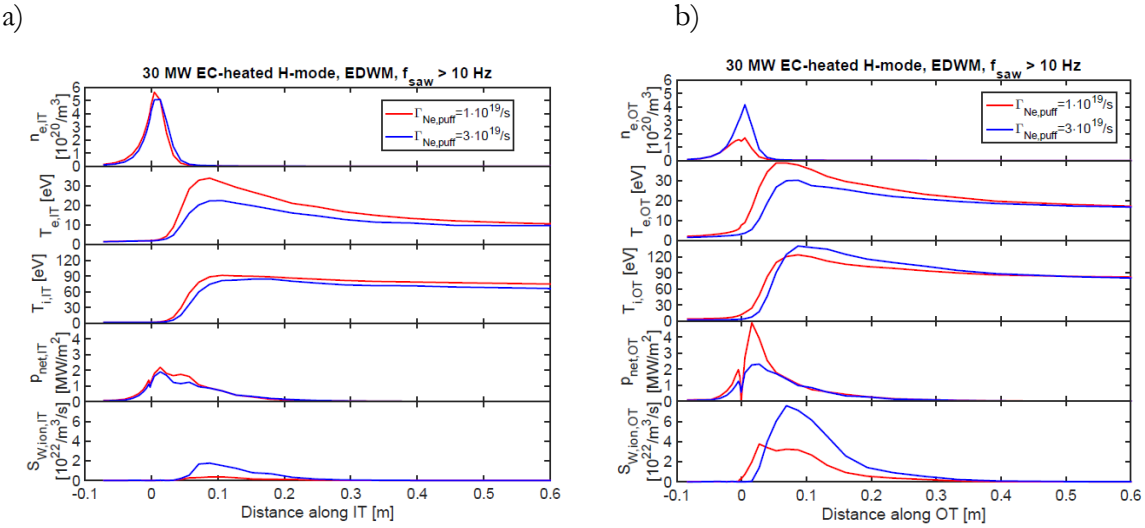

Figure 13. Divertor plasma density, electron and ion temperature, power flux and W source versus distance to the separatrix at the target for : a) the inner divertor and b) the outer divertor plasma of 5 MA/1.8T hydrogen H-modes with 30 MW ECRH heating power modelled with the

integrated self-consistent core-edge simulations with the EDMW model for core transport by JINTRAC [Militello-Asp 2018].

The results of these studies in Fig. 13 show that the divertor power flux at the outer divertor for low Ne levels are modelled to be very peaked (λ_q ~ 5 mm at the outer midplane) and its peak can reach values of ~ 5 MWm^{-2}. The electron temperature at the outer divertor target has maximum values of ~ 40 eV (this does not occur at the separatrix where the ion flux is the highest) for 30 MW ECH heated 5 MA/1.8T hydrogen plasmas in ITER. These levels of power loads and the resulting plasma parameters are in agreement with detailed SOLPS-ITER simulations for similar plasma conditions [Park 2019]. Increasing the level of Ne is effective in reducing the divertor power flux by a factor of ~ 2 in the simulations performed so far, which do not reach strongly detached divertor conditions at the outer divertor. The effective W sputtering yield for these plasmas is in the range of 0.0005 W-atom/H-ion (low Ne puffing rate case) to 0.001 W-atom/H-ion (high Ne puffing rate case) which is typical for W interacting with a hydrogenic plasma that contains a few % concentration of medium Z impurities and with a temperature of 10-20 eV [Kallenbach 2005]. The core W concentrations in these plasmas are very low (1.5-2.5 10^{-6}), as shown in Fig. 12.b, despite the fact that no local re-deposition of W is assumed in the simulations; this assumption results in a very conservative upper estimate of the W divertor source. The low core W concentration is due to the very effective screening of impurities in the pedestal plasma shown in Fig. 12.b. The effective screening of impurities in the ITER pedestal is caused by the neoclassical temperature screening term being dominant in low edge density gradient/high edge temperature gradient conditions at the ITER pedestal leading to an outwards-directed neoclassical impurity pinch velocity [Dux 2014]. Similar full-integrated simulations including ELM-resolved tungsten production and transport to core with JINTRAC are in progress and will be compared with those already performed with a simpler approach [Polevoi 2018].

The results of the studies of 5 MA/1.8T hydrogen H-mode stationary plasmas with 30 MW ECH heating show that there are no major operational physics-integration issues with respect to their practical feasibility in ITER. Many of the features of these H-mode plasmas will be similar to those of later phases in the ITER Research Plan narrow λ_q and high divertor power fluxes, impurity screening in the pedestal, etc. These H-mode scenarios can therefore provide a good basis for the development of ITER H-mode operation thus minimizing the risks associated with H-mode operation in later phases of the research plan.

6. Summary and Conclusions

The assessment detailed in this study identifies the plasma conditions for optimum H-mode access and sustainment in the PFPO-1 phase of the ITER Research Plan in which 20 MW of ECH will be available for plasma heating. With this level of additional heating H-mode access and sustainment of 5 MA/1.8 T H-mode plasmas is viable on the basis of the existing scalings and their physics-based extrapolation albeit only for helium plasmas and with a reduced operational space. Increase of the heating power level beyond the foreseen one in the baseline to 30 MW would open significantly the operational space of H-mode plasmas in helium and would allow the exploration of hydrogen or hydrogen dominant plasmas (i.e. hydrogen + 10 % helium) over a reduced operational space.

The H-mode plasma properties predicted by integrated modelling of deuterium plasma transport simulations with first principle models and pedestal-SOL parameters predicted by EPED1+SOLPS scalings is extrapolated to hydrogen operation. The simulations indicate central electron temperatures in excess of 10 keV with ion temperatures typically a factor of 2-3 times lower for H-mode plasmas with $n_e = 0.5\ n_{GW}$, for which H-mode sustainment is possible. Such difference between electron and ion temperatures is due to the central ECH heating of these plasmas depositing all additional heating power on the electrons and the

inefficient equipartition in the central region of the plasma due to the low absolute value of the plasma density (2-0-3.0 10^{19} m^{-3}). These first principle model predictions satisfactorily match results in JET and ASDEX-Upgrade experiments albeit at different collisionalities.

The comparison with low collisionality JET H-mode plasmas with a level of plasma current and additional heating similar to these ITER H-mode plasmas, scaled from JET to ITER following a dimensionless similarity approach, reveals good agreement in terms of global plasma energy and density and temperature profiles although not on the separate electron and ion temperature profiles. This is caused by differences in the heating schemes (ECH in ITER versus NBI in JET) and dominance of equipartition (low in ITER due to low densities and high in JET due to high densities). The characteristic scale lengths of the electron density and electron and ion temperatures for H-mode experiments at half radius in ASDEX-Upgrade with significant ECH heating are in line with those predicted for ITER, except the ion temperature profile predicted by GLF23 albeit, in contrast to ITER, in ASDEX-Upgrade the NBI power still constitutes 55% of the total additional power level heating mainly the ions.

Integration issues related to specific aspects of 5 MA/1.8 T H-mode operation in ITER have also been evaluated beyond the aspect of 3rd harmonic ECH heating, which is discussed in detail in [Schneider 2019]. These concern the impact of increased ripple at 1.8T on H-mode pedestal parameters, the consequences of uncontrolled ELMs on the tungsten divertor components and the magnitude of the divertor power fluxes and resulting core contamination by tungsten caused by plasma-wall interaction for these plasma conditions. It is estimated from extrapolation of experiments that TF ripple can have a significant effect on the achievable pedestal pressure decreasing the total plasma energy by 20-30%; this can be reduced by a factor of ~ 2 by modifying the plasma configuration and shifting the plasma radially inwards. Divertor and ELM power fluxes if uncontrolled are significant but well away from the limits determined by material limits (divertor macro-brush melting) and divertor stationary power exhaust for the ITER divertor design. Similarly, tungsten divertor production for hydrogen plasmas is not negligible but the favourable transport in the pedestal region (neoclassical screening) leads to very small levels of tungsten concentration in the main plasma as required for good H-mode confinement.

The results of our studies of 5 MA/1.8T hydrogen H-mode stationary plasmas with ECH heating show that these plasmas show many of the features of H-mode plasmas in later phases of the ITER Research Plan including integration issues with respect to their practical feasibility in ITER and, therefore, provide a good basis for the development of H-mode operation in ITER thus minimizing the risks associated with H-mode operation in later phases of the research plan. Some of the features of these plasmas are linked to the specific conditions of these operational scenarios in ITER such as the low density leading to low electron-ion equipartition and the increased level of ripple, and their impact on the plasma parameters and achievable confinement have been assessed on the basis of modelling results and comparison with experiments.

An important open issue to refine these quantitative evaluations concern the impact of the hydrogen isotope and/or plasma species (helium) on core plasma transport and overall confinement that can be achieved in H-mode. Many of the models used in our evaluations have been derived for deuterium plasmas (e.g. first principle transport models) and need to be refined to take into account different isotopes and/or different ion specifies since these are found to have non-negligible effects on H-mode access, pedestal stability and H-mode confinement in present experiments [Maggi 2018]. Note that temperature and density profiles predicted for 5MA/1.8T operation by GLF23, EDMW models match very well.

Acknowledgment: The authors are grateful to C. Angioni, C. Bourdelle, H. Urano, G. Staebler, J. Citrin and the members of the International Tokamak Physics Activities Transport and Confinement group for enlightening discussions and advice.

Disclaimer: ITER is the Nuclear Facility INB no. 174. The views and opinions expressed herein do not necessarily reflect those of the ITER Organization.

References

[Aiba 2011] N. Aiba, et al., Nucl. Fusion **51** (2011) 073012.

[Andrew 2006] Y Andrew, et al., Plasma Phys. Control. Fusion **48** (2006) 479.

[Andrew 2008] Y. Andrew et al., Plasma Phys. Control. Fusion **50** (2008) 124053.

[Angioni 2009] C Angioni et al 2009 Plasma Phys. Control. Fusion **51** 124017.

[Artola 2008] F.J. Artola, et al., Nucl. Fusion **58** (2018) 096018.

[Beurskens 2009] M. N. A. Beurskens, et al., Plasma Phys. Control. Fusion **51** (2009) 124051.

[Bigot 2019] B. Bigot, Nucl. Fusion **59** (2019) 112001.

[Bourdelle 2014] C. Bourdelle, et al., Nucl. Fusion **54** (2014) 022001.

[Chapman 2012] I.T. Chapman, et al., Nucl. Fusion **52** (2012) 063006.

[Dux 2014] R. Dux, et al., Plasma Phys. Control. Fusion **56** (2014) 124003.

[Eich 2017] T. Eich, et al., Nuclear Materials and Energy **12** (2017) 84.

[Futatani 2014] S. Futatani, et al., Nucl. Fusion **54** (2014) 073008.

[Gohil 2008] P. Gohil, et al, Journal of Physics: Conference Series **123** (2008) 012017.

[Gohil 2012] P. Gohil et al., Proc. 24th IAEA Fusion Energy Conf. (San Diego, USA, 2012), ITR/P1-36.

[Gunn 2017] J.P. Gunn, et al., Nucl. Fusion **57** (2017) 046025.

[Hillesheim 2016] J. Hillesheim et al., Proc. 26th IAEA Fusion Energy Conf. (Kyoto, Japan, 2016) EX/5-2.

[IRP 2018] ITER Research Plan. ITR-18-03, ITER Organization 2018.

[Kallenbach 2005] A. Kallenbach, et al., Plasma Phys. Control. Fusion **47** (2005) B207.

[Kallenbach 2013] A. Kallenbach, et al., Plasma Phys. Control. Fusion **55** (2013) 124041.

[Li 2020] L. Li, et al., Nucl. Fusion **60** (2020) 016013.

[Loarte 2003] A. Loarte, et al., Plasma Phys. Control. Fusion **45** (2003) 1549.

[Loarte 2014] A. Loarte, et al., Nucl. Fusion **54** (2014) 033007.

[Lukash 2017] V.E. Lukash, et al., 44th EPS Conf. on Plasma Physics, Belfast, United Kingdom, 2017, paper P5.152 (http://ocs.ciemat.es/EPS2017PAP/pdf/P5.152.pdf).

[Maggi 2014] C.F. Maggi, et al, Nucl. Fusion **54** (2014) 023007.

[Maggi 2018] C. F. Maggi, et al., Plasma Phys. Control. Fusion **60** (2018) 014045.

[Martin 2008] Y.R. Martin et al., J. of Phys. Conf. Series **123** (2008) 012033.

[Mc Donald 2010] D.C. McDonald et al., Proc. 23rd IAEA Fusion Energy Conf. (Daejeon, Korea, 2010) EXC/2-4Rb.

[Militello-Asp 2018] E. Militello-Asp, et al., Proc. 60th Annual Meeting of the APS Division of Plasma Physics, 2018, Portland, USA, paper UO5.00008.

[Nunes 2013] I. Nunes, et al., Nucl. Fusion **53** (2013) 073020.

[Park 2019] J. S. Park, et al., Proc. 61st Annual Meeting of the APS Division of Plasma Physics Fort Lauderdale, USA, paper PO5.00012.

[Pereverzev 2002] G.V. Pereverzev and P.N. Yushmanov, "ASTRA Automated System for TRansport Analysis in a Tokamak," Max-Planck IPP Report, vol. 5/98, 2002, https://w3.pppl.gov/~hammett/work/2009/Astra_ocr.pdf.

[Polevoi 2003] A.R. Polevoi, et al, Nucl. Fusion **43** (2003) 1072.

[Polevoi 2017] A.R. Polevoi, et al., Nucl. Fusion **57** (2017) 022014.

[Polevoi 2018] A.R. Polevoi, A. Loarte, et al, Nucl. Fusion **58** (2018) 056020.

[Righi 1999] E. Righi et al., Nucl. Fusion **39** (1999) 309.

[Ryter 2013] F. Ryter et al., Nucl. Fusion **53** (2013) 113003.

[Ryter 2014] F. Ryter et al., Nucl. Fusion **54** (2014) 083003. M. Schmidtmayr et al 2018 Nucl. Fusion 58 056003.

[Saibene 2008] G. Saibene, et al., Proc. 22nd IAEA Fusion Energy Conf. (Geneva, Switzerland, 2008) EX/2-1.

[Schmidtmayr 2018] M. Schmidtmayr, et al., Nucl. Fusion **58** (2018) 056003.

[Schneider 2019] M. Schneider et al., Nucl. Fusion **59** (2019) 26014.

[Solano 2019] E.R. Solano, et al., Proc. 61st Annual Meeting of the APS Division of Plasma Physics, Fort Lauderdale, USA, 2019, paper PO5.002.

[Sommer 2015] F. Sommer, et al., Nucl. Fusion **55** (2015) 033006.

[Staebler 2007] G. M. Staebler, et al., Physics of Plasmas **14** (2007) 055909.

[Staebler 2017] G.M. Staebler, et al., Nucl. Fusion **57** (2017) 066046.

[Strand 2004] P. Strand, et al., Proc. 31st EPS Plasma Physics Conference, London, United Kingdom, 2004, ECA Vol. 28G, P-5.187.

[Takizuka 2004] T. Takizuka, et al., Plasma Phys. Control. Fusion **46** (2004) A22.

[Tobita 1995] K. Tobita et al., Nucl. Fusion **35** (1995) 12.

[Urano 2011] H. Urano, et al., Nucl. Fusion **51** (2011) 113004.

[Waltz 1997] R.E. Waltz, et al., Physics of Plasmas **4** (1997) 2482.

[Yan 2016] Z. Yan, et al., 26th IAEA Fusion Energy Conference Kyoto, Japan, 2016, paper EX-5-1.